Demonstrating the Potential of Low-Cost GPS Units for the Remote Measurement of Tides and Water Levels Using Interferometric Reflectometry

SIMON D. P. WILLIAMS,[a] PAUL S. BELL,[b] DAVID L. MCCANN,[c] AND RICHARD COOKE

National Oceanography Centre, Liverpool, United Kingdom

CHRISTINE SAMS

National Oceanography Centre, Southampton, United Kingdom

(Manuscript received 30 April 2020, in final form 13 July 2020)

ABSTRACT: A low-cost [$30 (U.S. dollars)] consumer grade GPS receiver with a sideways-mounted antenna has been applied to measure tidal water levels at a mesotidal coastal site using an interferometric reflectometry approach. The proof-of-concept system was installed approximately 16 m above mean sea level in close proximity to a conventional bubbler tide gauge that provided validation data. The received signal-to-noise ratios (SNR) for the satellites in view were recorded for several months during two successive years and the observed frequencies of the interferometric oscillations used to calculate the difference in elevation between the receiver and the water surface. Comparisons with concurrent and historic in situ tide gauge data at the site initially helped to identify a calibration issue with the in situ gauge. The GPS-based measurements were shown to be in excellent agreement with the corrected in situ gauge, exhibiting a root-mean-square difference of 5.7 cm over a tidal range exceeding 3 m at spring tides and a daily averaged RMS of 1.7 cm. The SNR data from the low-cost GPS receivers are shown to provide significantly higher-quality data for this purpose compared with high-end geodetic grade receivers at similar sites. This low-cost, widely available technology has the potential to be applied globally for monitoring water levels in a wide variety of circumstances and applications that would otherwise be cost or situation prohibitive. It could also be applied as an independent cross check and quality control measure for conventional water-level gauges.

KEYWORDS: Ocean; Global positioning systems (GPS); In situ oceanic observations; Measurements

1. Introduction

The measurement of water levels over sustained periods of time can be a logistically and financially significant commitment for any organization. Conventional water-level measurements either require equipment to be in the water, such as pressure- and bubbler-based systems, or directly over the water such as radar gauges. In-water gauges are prone to corrosion and are often sited in busy port locations where all types of gauge are susceptible to direct physical damage. If sited in insecure but populated locations the risk of theft and vandalism must be considered by operators.

Depending on the intended data application and quality required of the installation, hardware and installation costs for even temporary water-level gauges can easily run to mid–tens of thousands of U.S. dollars when surveys, installation design, hardware, electrical supply and staff time are all factored in. Long-term operation of water-level gauges is an even more significant challenge as consideration must also be given to the long-term stability/calibration of measurements, monitoring for possible vertical land movements, quality control of data and appropriate data archiving provisions [Intergovernmental Oceanographic Commission (IOC); IOC 2006].

These multiple factors place the resources and capability to install and maintain such systems within the grasp of only the largest and most sustainably funded projects and organizations.

Ground based global positioning system (GPS) and Global Navigation Satellite Systems Interferometric Reflectometry (GNSS-IR) is a fairly recent technique that allows you to monitor some aspects of the state of the environment around a GNSS antenna by understanding the patterns derived from the interactions of the direct and reflected signals. The signal-to-noise ratio (SNR) was shown by Axelrad et al. (1996) to be useful for characterizing multipath signals and amplitudes. Given a simple geometry of a planar surface below a GNSS antenna, Georgiadou and Kleusberg (1988) and Elosegui et al. (1995) showed that the interference patterns had a distinct frequency that was related to the height of the antenna above

[a] ORCID: 0000-0003-4123-4973.
[b] ORCID: 0000-0002-4673-4822.
[c] ORCID: 0000-0003-4428-700X.

Denotes content that is immediately available upon publication as open access.

Supplemental information related to this paper is available at the Journals Online website: https://doi.org/10.1175/JTECH-D-20-0063.s1.

Corresponding author: Simon Williams, sdwil@noc.ac.uk

DOI: 10.1175/JTECH-D-20-0063.1

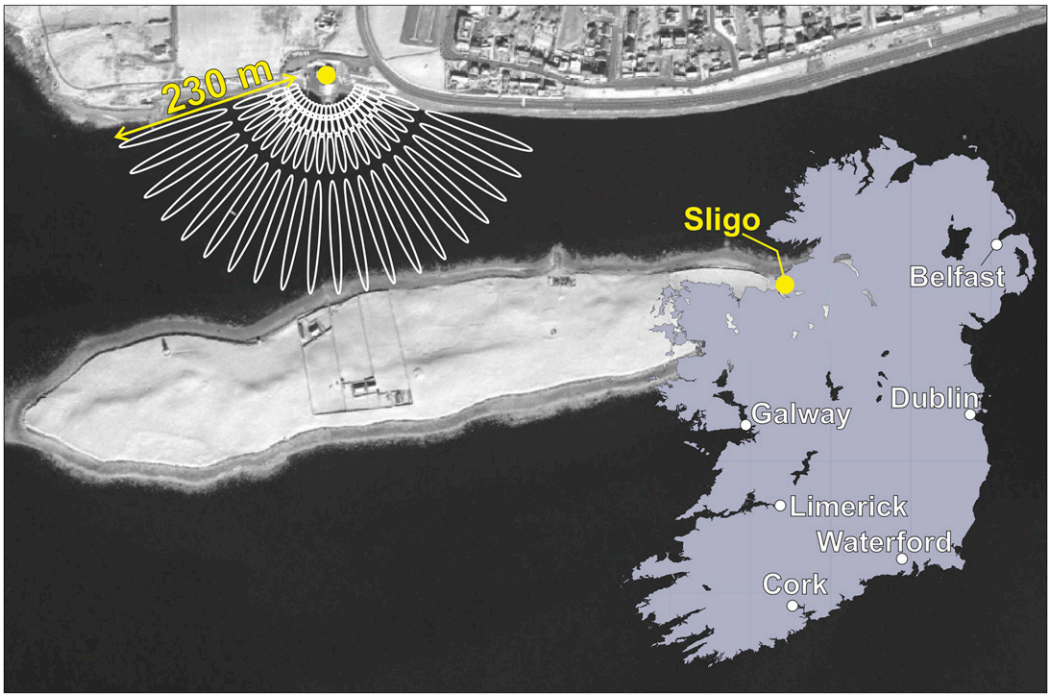

FIG. 1. Satellite view of the Sligo test site (solid yellow circle) with Fresnel zones for a reflector height of 16 m and elevation angles of 5° (largest white ellipses), 10°, 15°, and 20° (smallest ellipses) within the azimuth range 110°–251°.

the surface. The first demonstration of water levels derived from GPS interferometric reflectometry (GPS-IR) SNR measurements was in Onsala, Sweden (Larson et al. 2013). Since then there have been many studies covering various aspects such as precision and accuracy of the retrievals (e.g., Strandberg et al. 2016; Santamaría-Gómez and Watson 2017; Santamaría-Gómez et al. 2015), tropospheric delay (Williams and Nievinski 2017), and the use of multiple satellite systems (e.g., Jin et al. 2017; Löfgren and Haas 2014). Santamaría-Gómez and Watson (2017) mounted a geodetic-quality antenna sideways and oriented in azimuth to face the sea and found a much clearer signal lasting to higher elevations than a conventionally upright-mounted antenna. The results from the sideways-mounted antenna were found to have a threefold increase in precision compared to the upright antenna. A 10-yr comparison at Friday Harbor, Washington, between a GPS-IR analysis and collocated tide gauge showed daily averages to be in agreement at the 2-cm level (Larson et al. 2017). One thing that is common to all these studies is the use of a high-end geodetic-quality antenna and receivers with an associated cost in the tens of thousands of U.S. dollars and all but a few were installed for the purpose of positioning/timing and not for GNSS-IR purposes.

Here we describe the recent demonstration of a low-cost water-level measurement system based on a basic consumer grade GPS receiver that requires a slightly elevated position close to and with clear line of sight to the water. The low-cost nature of such systems opens up the possibility of using multiple examples of such gauges for applications as diverse as tide gauges, lake and river level monitoring, flood plain inundation, snow and ice depth and possibly even localized progressive subsidence, e.g., around developing sinkholes. The small physical size of the receiver antenna lends itself to relatively unobtrusive installation and thus a reduced risk of vandalism and damage in insecure environments.

While at present we would not advocate the replacement of more conventional water-level systems with these low-cost solutions, the example shown here already demonstrates the value of such an approach for identifying potential issues with the data from conventional systems if used in tandem.

2. Instrumentation and deployment

As part of a collaboration with the Royal National Lifeboat Institution (RNLI) to demonstrate low-cost, real-time sea level measurements for intertidal public safety we installed our trial system at the Sligo RNLI station in Ireland (Fig. 1). Public access to the nearby Coney Island (Inishmulclohy, which is west and southwest of the island shown in Fig. 1) is via a causeway (Cummeen Strand) at low tide and therefore a major source of safety incidents for the RNLI station. A real-time sea level measurement system would help to alleviate incidents by providing better information than the current ''Text the Tide'' system that delivers safe crossing times via text message and relies on tidal predictions from a nearby gauge (not the one recently installed at the site). This system only operates during summer months as meteorological influences during winter cause unacceptable deviations from the harmonically predicted tides, making the prediction of safe crossing times for the causeway problematic. Better information on water

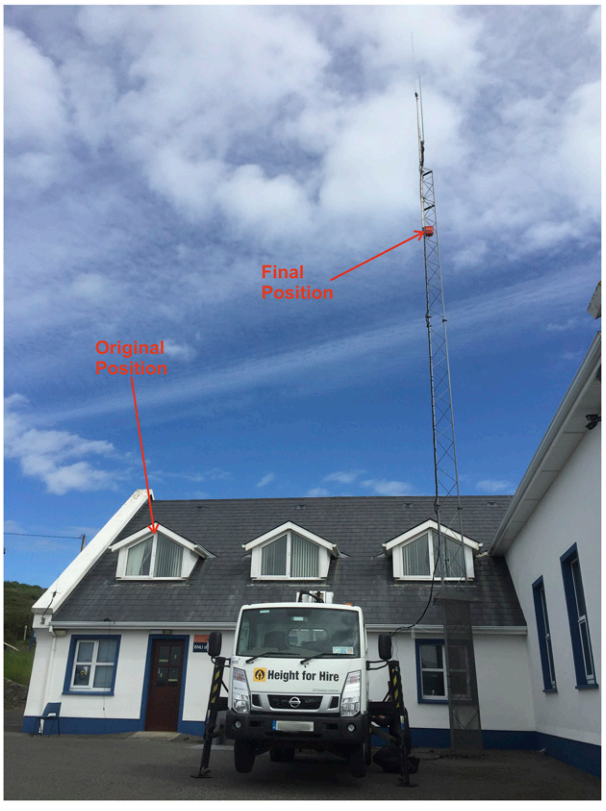

FIG. 2. Northward view of the RNLI Station at Sligo, Ireland. The labels indicate the original and final locations of the GPS antennas.

levels would also provide the RNLI crew with more insight into the likely water depths to expect over the sand flats and sand banks when conducting rescues.

The GPS receiver for the system was initially installed at the apex of the top-left window (Fig. 2, left) for ease of access to the logging computer. However, preliminary analysis of the data recorded from this position showed that although the receiver was working, it had a limited view of the water which was far from optimal. The receiver was subsequently moved to a more elevated position on the adjacent radio mast (Fig. 2, right). The view of the water from the new position is shown in Fig. 3. All data presented in this paper are from the position of the radio mast; the earlier data from the window have not been included in this study.

The original GPS receiver was a low-cost [$30 (U.S. dollars)] USB puck unit comprising a Globalsat BU353S4 that uses the SiRFstar IV receiver with a patch antenna, coupled with two daisy-chained 15-m USB extender cables needed to link the receiver at the new location on the mast back to the logging computer inside the building. These were secured as a temporary measure using PVC tape. We recorded data from 18 June through 1 August 2018 with a gap of 10 days when the logging PC crashed. This system proved insufficiently robust for long-term installation in the local environment and communications with the GPS unit failed later that summer. However, the proof of concept provided data of sufficient quality to justify a second deployment.

In spring 2019 we replaced the GPS receiver with a Maestro A2200A SiRFstar IV module allowing us to use a continuous weatherproof power cable and link the serial receiver output to an XBee wireless telemetry system for short range transmission from the mast back to the building. The wireless telemetry enabled the power supply wiring to be decoupled from the logging and display computer, thus allowing that computer to be moved around the building at will. The small weatherproof plastic box containing this system, and with the GPS receiver and antenna mounted inside the plastic box, was more securely fixed to the tower's metal lattice but at a slightly different height due to the availability of suitable fixing points. This unavoidably led to an offset in the mean level of our reflector height estimates between the two years. Project resources were unfortunately not sufficient to cover a levelling exercise to independently establish the change in heights of the antennas. A further 83 days of data from 22 May to 13 August 2019 were logged using this new system, and the system continues to operate at the time of writing.

In both cases we recorded the CN0 signal (SNR) at 1-s intervals for all available satellites. The receivers only record data from the U.S. GPS navigation system and only on the L1 frequency (1575.42 MHz). Recent geodetic-quality GNSS receivers can typically record data from all current GNSS systems (e.g., GPS, Glonass, Galileo and BeiDou) and multiple frequencies, significantly increasing the amount of sea level retrievals available per day. In this study, the receiver's antenna was mounted sideways and pointing toward the water surface. In previous work, Santamaría-Gómez and Watson (2017) mounted a geodetic-quality antenna sideways to increase the range of elevations where a strong SNR interferometric signal is obtained. Our reasoning for mounting the

FIG. 3. Panoramic view from the GPS antenna of the water surface. Note the island, hills in the distance that will limit observations at very low (<5°) elevations, and the possible clutter due to the two piers at higher azimuths. The OTT tide gauge is installed at the end of the far pier.

antenna horizontally was different; low-cost receivers typically measure, simultaneously, fewer satellites than a geodetic-quality receiver can, and we hoped that pointing the antenna in the direction of the water surface we could maximize the recording of those in that direction. However, subsequent analysis of the satellites recorded failed to show any preferential recording from that direction. The same strengthening of the signal may also result from mounting the low-cost antenna sideways.

For comparison there is a continuously operating tide gauge at Sligo (Rosses Point) maintained by Marine Ireland which consists of an OTT Hydrometry compact bubble sensor (CBS). The tide gauge is mounted on a pier around 60 m southwest of the GPS sensor. Six-min data with occasional gaps are available from October 2017. Data are also publicly available from January 2010 to August 2013 as hourly averages.

3. Data analysis and results

There are a variety of methods and experimental arrangements to measure water levels using GPS. Here we focus on ground based GPS-IR which uses the measured SNR as a function of satellite elevation as the primary observable (Bilich et al. 2007; Larson et al. 2013; Löfgren and Haas 2014; Löfgren et al. 2014). Elevations and azimuths of the GPS satellites are calculated using the broadcast ephemerides. The interference between the direct and reflected signal from a flat surface produces a periodic signal that is related to the elevation angle, the wavelength of the signal λ (for the GPS L1 frequency the wavelength is 19.04 cm), and reflector height (H, the height of the reflecting surface below the antenna). In its simplest form this can be modeled as

$$\mathrm{SNR}(e) = A_d(e) + A(e)\cos\left[\frac{4\pi H}{\lambda}\sin(e) + \phi\right], \qquad (1)$$

where $A_d(e)$ is the direct signal contribution which is a function of satellite antenna power and the receiving antenna gain pattern; $A(e)$ is the multipath amplitude, which can be elevation and time dependent (see Nievinski and Larson 2014), but for our purpose we can assume to be constant; e is the satellite elevation angle with respect to the horizon; and ϕ is a phase constant. Spectral analysis of this signal should yield a peak at a frequency that is related to H. Although the measurements are evenly recorded in time (in this case 1 Hz) the elevation angles e are not so we use a Lomb–Scargle periodogram (LSP; or simply periodogram hereinafter) (Lomb 1976; Scargle 1982) with an oversampling factor to yield a nominal precision of 1 mm. Prior to using the periodogram the direct signal is removed using a low-order polynomial (or equivalent) and converted to a linear scale (V) from units of dB Hz.

Each satellite pass is split into separate ascending and descending arcs and we mask out arcs that do not sense the water based on a range of azimuth and elevation angles. The remaining arcs allow us to calculate the water level at various times of the day. Note that the repeat times of the GPS satellite positions are approximately 4 min shorter than 1 day, so this, coupled with the orbital geometries, leads to uneven sampling times. The average length of an arc in this experiment is around 45 min. Over this time the reflecting surface is likely to be nonstationary and this will shift the spectral peak by

$$\dot{H}\frac{\tan e}{\dot{e}}, \qquad (2)$$

where $\dot{e}$ and $\dot{H}$ are the time derivatives of e and H. If we are trying to estimate H, then we also do not know $\dot{H}$. We take the approach described in Larson et al. (2017) where we initially ignore $\dot{H}$ and then directly solve for this effect during a tidal analysis assuming that the biggest contributor to the changing reflector height is the diurnal and semidiurnal tides.

Figure 1 illustrates the reflection mask we employed in this study. The ellipses shown represent the GPS-IR footprints (also called Fresnel zones) for a range of elevations and azimuths for a nominal height of 16 m above sea level. The azimuth range shown is from 110° to 251° and the elevations are 5°, 10°, 15°, and 20°. The outermost semicircle of ellipses represent the 5° elevation angles and the innermost 20° elevations. Note there is some overlap with the coast in these ellipses at the edges of the azimuth range for higher elevations. So to reduce the contamination of the SNR signal from the land and the piers to the southwest of the antenna, we used an inner mask between 117° and 120° with an elevation range of 10°–20° and an outer mask with an elevation range of 5°–12° to either side. Any noisy SNR signals due to multipath from non-water-surface reflections on the edges are likely to be picked up in the postprocessing quality control.

The propagation delay due to the neutral atmosphere will also manifest itself in GNSS-IR measurements as a height bias (Santamaría-Gómez and Watson 2017; Williams and Nievinski 2017). We directly apply a correction during the periodogram calculation using the VMF1 mapping function (Böhm et al. 2006) together with the Global Temperature and Pressure (GPT2w) model (Böhm et al. 2014) as described in Williams and Nievinski (2017) to account for this error.

An example SNR plot of a satellite arc from our site and its periodogram is shown in Fig. 4 (bottom). Also shown are equivalent SNR and periodogram plots for the same satellite arc (PRN 13) on the same day at two sites, BRST in Brest (Fig. 4, top), France and ACOR, in A Coruña, Spain (Fig. 4, middle). Both sites have geodetic-quality antennas and receivers installed, are at a similar height above mean sea level, have a sizeable tidal range and are not too dissimilar in their local environment to Sligo. At the time of measurement, a Trimble Alloy receiver with a Trimble Zephyr 2 base antenna (TRM57971.00 NONE) was installed at BRST and at ACOR a Leica GR10 receiver was coupled with a Leica choke ring antenna (LEIAT50 LEIS). We see that the periodic signal (indicative of a reflection off a flat, coherent surface) is clearer at Sligo than both BRST and ACOR and extends over a larger elevation range. These effects were also noted by Santamaría-Gómez and Watson (2017) where they mounted a geodetic-quality receiver sideways at Spring Bay, Tasmania, Australia. The periodogram (Fig. 4, right) shows that the peak power at Sligo is over 3 times larger than at BRST or ACOR so, along with the extended elevation range, could be expected to produce a more precise estimate of reflector height. Typically,

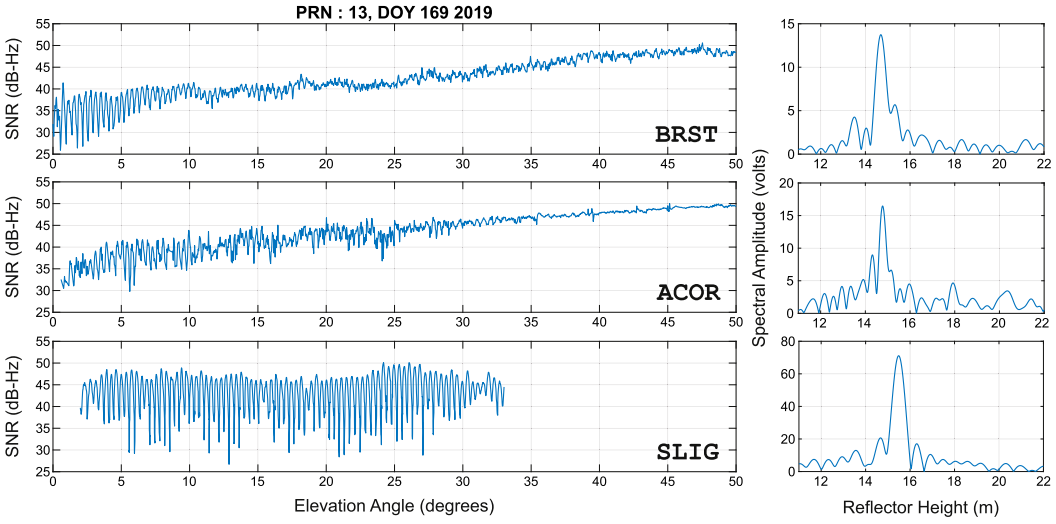

FIG. 4. (left) Example of SNR vs elevation angle for PRN 13 on DOY 169 during 2019 at three sites: BRST (top) Brest, France (BRST); (middle) A Coruña, Spain (ACOR); and (bottom) Sligo, Ireland (SLIG). (right) Periodograms for these records. Note the difference in scale on the *y* axes of the right panels.

we expect zenith-mounted geodetic-quality receivers to be less sensitive to reflected signals because the antenna gain pattern and the ground plane are designed to reduce multipath at low elevation angles. There are probably two main reasons why we see an extended elevation range and larger peak power, the orientation of the antenna sideways and pointing toward the sea or the lack of multipath immunity with such a cheap antenna or both. We did not test the antenna in a vertical orientation, as this was a practical field test, to ascertain which was the major contribution.

In total there were 2930 height estimates from individual ascending/descending satellite arcs, of which 27 were removed because the estimated reflector height was below a minimum set at 14 m. We then performed an iterative quality control whereby we fitted tidal parameters using least squares harmonic estimation (e.g., Foreman and Henry 1989; Foreman and Neufeld 1991; Foreman et al. 2009), and adapted to account for the $\dot{H}$ effect [see Larson et al. (2017) for details], and then fit a piecewise cubic B-spline with $6n$ knots, where n is the number of days with measurements. The knots were not evenly spaced in time, instead they were evenly spaced in measurements. We found that our choice of $6n$ knots was a good compromise, after testing, between over and underfitting with the B-spline for outlier removal. The B-spline was only used as an internal approach to outlier removal, that is, without the use of external information such as the bubbler tide gauge. We removed the B-spline from the tidal residuals and estimated a *t* location–scale distribution. Outliers were then removed that were more than 3 times the scale parameter. A *t* location–scale distribution, which is a generalization of Student's *t* distribution to include location and scale parameters, was chosen as it is useful for modeling a data distribution with heavy tails (outliers) while approaching the normal distribution as the shape parameter increases. This whole procedure was repeated three times. A further 106 outliers were removed at this point giving a retrieval rate of 95.5%. We end up with a median of 32 and 21 measurements per day for the 2018 and 2019 subsets, respectively. We do not know why the 2019 data with the Maestro receiver gave us less data. However, these are still comparable to the mean observations per day found by Löfgren et al. (2014) of between 14 and 210 at five GPS sites around the world. The final H time series is shown in Fig. 5. The $\dot{H}$ effect has not been accounted for in this plot but the tropospheric delay has since it is directly applied in the processing. We see a very obvious tidal effect with a range of around 3–4 m. The residuals after fitting the tidal parameters and accounting for the $\dot{H}$ effect are shown in Fig. 6. We can clearly see residual long-period variations on the order of 20–40 cm are visible. After removing the piecewise cubic B-spline we get an internal estimate for the sample standard deviation of 4.6 cm. A better comparison is with a collocated tide gauge which we show in the next section.

4. Comparison with collocated tide gauge

The equivalent residuals from the collocated bubbler gauge are also shown in Fig. 6 (orange). We see very similar fluctuations in both sets of residuals but also some long-period differences between the two. Although the absolute level of the residual heights is arbitrary, both series have had the tidal predictions and a mean value removed, we see that in 2018 the bubbler gauge residuals start off lower than the GPS-derived residuals but are closer at the end of July and in 2019 the bubbler gauge residuals are higher than the GPS-derived residuals at the end of the series. There can be several explanations for this. First, there was a change in the GPS antenna/receiver between the 2 years and after swapping, the system was installed slightly higher on the radio mast, so we can expect an offset between the 2 years. In fact we calculate this offset to be 20.4 ± 0.2 cm which if corrected (in Fig. 8) would bring the 2018 and 2019 GPS residuals down and up, respectively, by

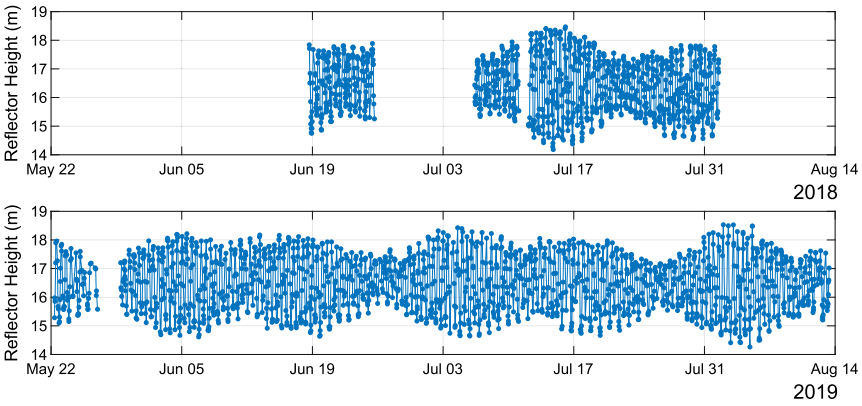

FIG. 5. Time series of estimated reflector heights for (top) 2018 and (bottom) 2019. The $\dot{H}$ effect has not been removed at this point.

approximately 10 cm, enhancing the fit. Second, we only have 117 days (and 2733 observations) of GPS derived heights spread over just over one year in order to estimate the tidal parameters compared to 622 days (~150 000 observations) of bubbler gauge measurements over 2 years. The tidal parameters from the GPS derived observations are likely not well constrained particularly for some of the longer period harmonics, which would lead to the differences seen.

Another useful way to compare tide gauge data is to use a Van de Casteele diagram (Martín Míguez et al. 2008, 2012) as it can highlight issues such as time keeping errors and scale problems among others (Pérez et al. 2014). The Van de Casteele plots the difference between the GPS and bubbler gauge–derived heights on the x axis and the sea level heights along the y axis. In this case the $\dot{H}$ effect and the offset has been removed in the GPS derived heights prior to differencing with the bubbler gauge measurements. The bubbler gauge measurements have been interpolated onto the times of the GPS measurements. The results are shown in Fig. 7 (left). A wide limit of −1 to 1 m was chosen in the x axis so as not to make the results look better but to compare with similar Van de Casteele diagrams in Löfgren et al. (2014) (cf. their Fig. 9). Since the GPS derived heights refer to the antenna phase center and the bubbler gauge measurements to a chart datum an offset in the x direction is entirely arbitrary and therefore of no importance here. The slope indicates a scaling issue, i.e., that either the range of the GPS derived heights is too small or that the range of the bubbler gauge heights is too large. We estimate this scaling factor to be 0.9721 ± 0.001, that is, $H_{\mathrm{gps}} = 0.9721 H_{\mathrm{tg}}$, where H_{gps} and H_{tg} are the GPS and tide gauge heights. The middle plot of Fig. 7 shows the results after correcting the scaling issue. We have a root-mean-square error (RMSE) of 5.7 cm. Williams and Nievinski (2017) showed that the tropospheric delay could produce a similar scaling error of a similar size but we have already accounted for that in our processing. So either there is another scaling issue in the GPS heights, our tropospheric correction is wrong or there is an issue in the tide gauge data. There is some evidence to suggest that it is the tide gauge data that have a scaling issue. As mentioned above we also have an earlier dataset from the same location. We cannot compare the two datasets directly as they do not overlap in time but we can compare the tidal predictions (Fig. 7, right). We see a similar scaling issue. Again this could be a problem in either of the sets but if we look at the estimated amplitudes of

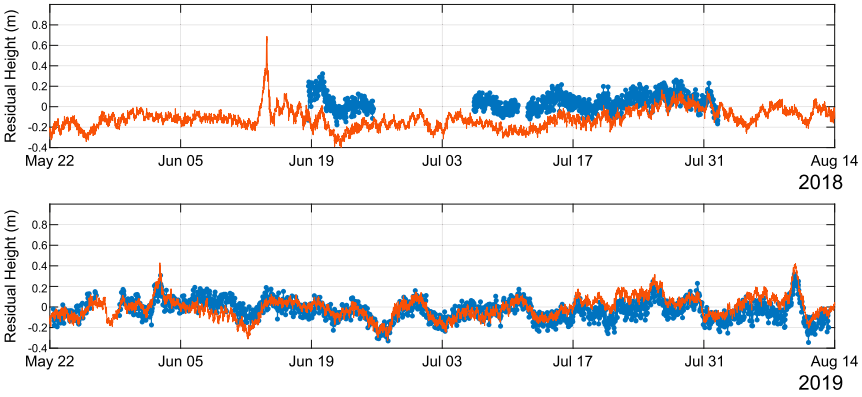

FIG. 6. Time series of residual heights for (top) 2018 and (bottom) 2019 after tides have been removed. Also shown are the residuals from the collocated tide gauge (orange). Tides for both series have been estimated separately. The $\dot{H}$ effect has been removed at this point.

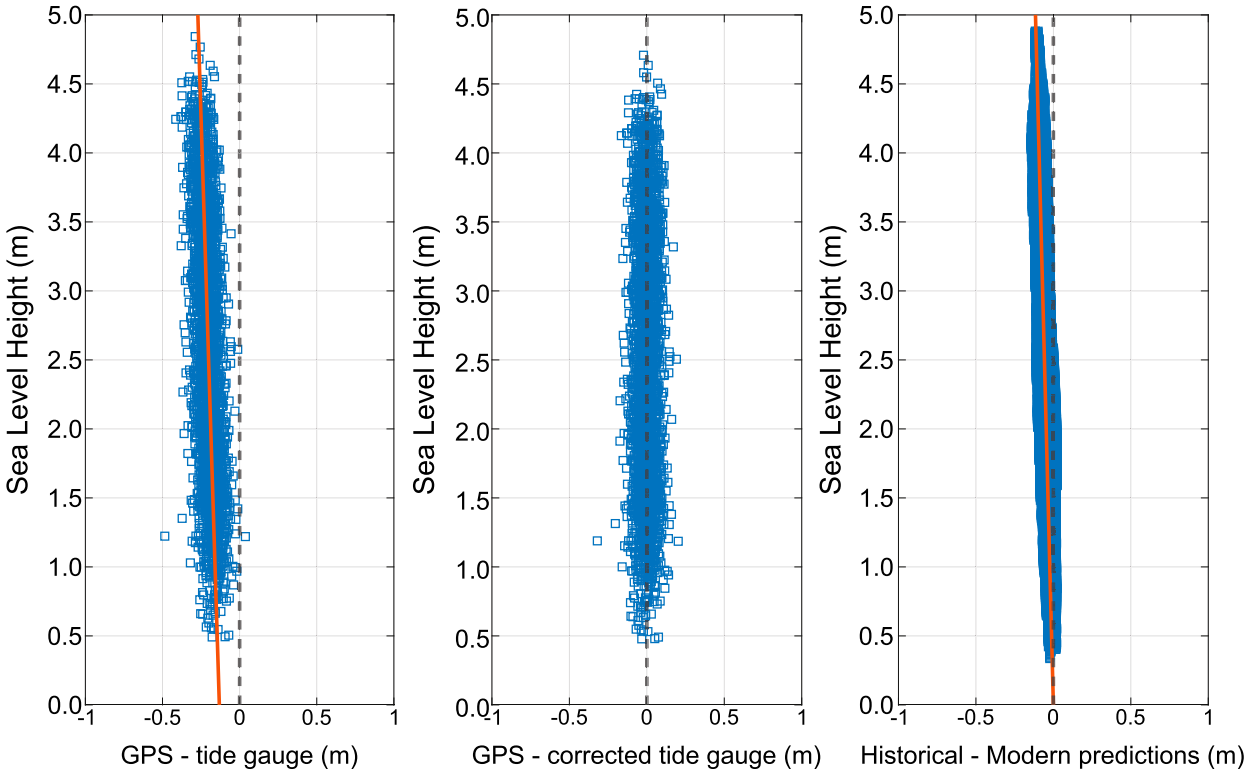

FIG. 7. (left) Van de Casteele diagram of the differences between the GPS and OTT CBS tide gauge as a function of the water level. The offset is arbitrary as the two datasets are not referenced to a common height. There is an obvious scaling error as a function of water level. The orange line is a fit to this scaling error. (center) Scaling-corrected Van de Casteele diagram. (right) Van De Casteele diagram of the differences between the predictions based on the historical (2010–13) and the modern (2017–present) tide gauge records. A similar scaling problem can be seen. The $\dot{H}$ effect has been removed at this point.

the main tidal constituent here, M_2, the amplitudes are 123.7, 120.4, and 119.5 cm for the modern tide gauge, historical tide gauge and GPS heights, respectively (with respective phases of 160.0°, 159.9°, and 160.1°). The historical tide gauge amplitude is much closer to the GPS result than the modern gauge. If we scale the modern M_2 amplitude by 0.9721 we get 120.2 cm. It is possible that the tidal amplitudes can change with time (Woodworth 2010; Müller et al. 2011; Haigh et al. 2020) but if we split up the (albeit limited) tide gauge data into smaller sections (yearly for historical, two sections for the modern) the variation in the amplitudes are on the order of a few mm compared to the 3.3-cm difference in amplitude between the two sections. Furthermore, the scale factor of 0.9721 is close to what you would get if the tide gauge was mistakenly set up to calculate height from pressure using a freshwater ($\sim$1000 kg m^{-3}) instead of seawater density (around 1023–1028 kg m^{-3}) (see online supplemental material for further verification). The GPS-IR and bubbler gauge residuals are plotted again in Fig. 8. This time we use the tidal predictions from the historical bubbler gauge measurements, scale the modern bubbler gauge measurements and remove the offset between the 2018 and 2019 subsets. We see a much improved fit over Fig. 6. We find the daily averages between the two datasets to be in agreement at the 1.7-cm RMSE level, slightly lower or equivalent to the 10-yr comparison by Larson et al. (2017).

5. Discussion and conclusions

The results shown above, together with the comparison with the collocated tide gauge, show that the low-cost antenna is capable of measuring water levels leaving the question of how the results from a low-cost receiver compares to results from geodetic-quality receivers. It is potentially difficult to quantify this as there are many factors that go into the accuracy of the measurements at a particular site, for instance, the local environment, the equipment used (antenna, receiver, and firmware), the settings applied (frequency of measurements and the resolution of the SNR values recorded), and the method used to estimate the water level. The local environment is most likely the major contributor to accuracy and includes such things as height of the instrument above the water, local multipath signals other than the water (harbor vs urban vs non-urban settings), sea state (a harbor could act as a stilling well compared to open ocean), and sky/water view (distant topography blocking low elevation angles and location of antenna away from water's edge limiting high elevation angles). Tidal range may also be a contributing factor, as suggested by Löfgren et al. (2014), primarily as a result of the application of

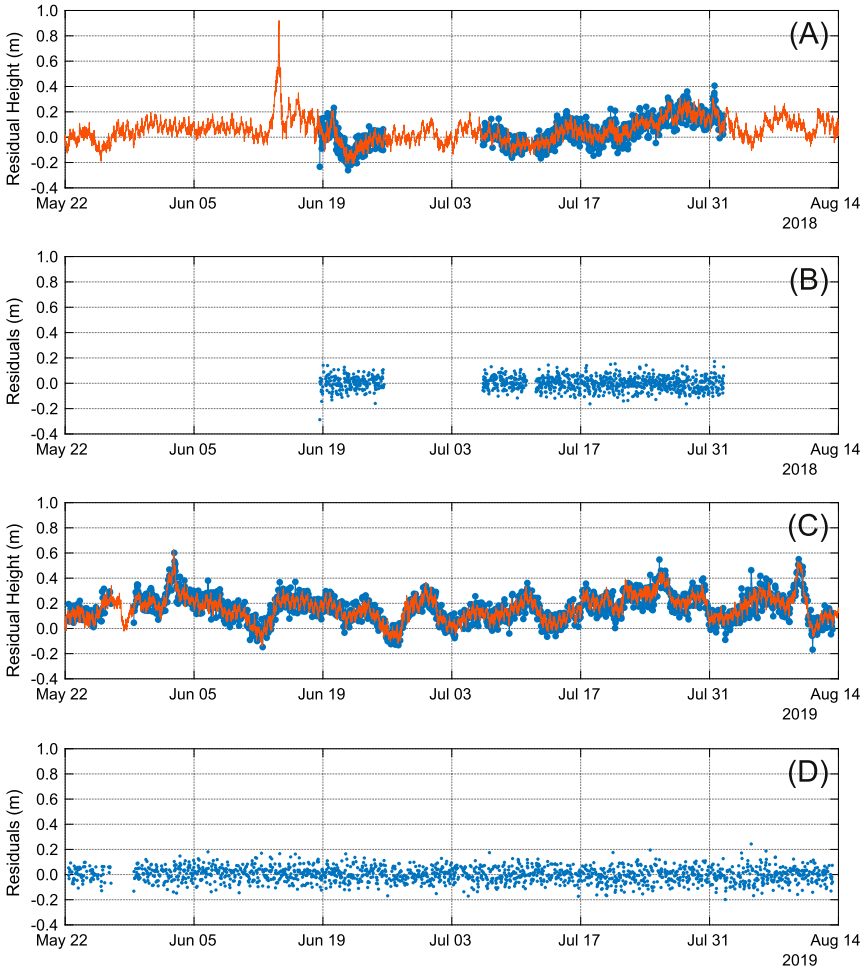

FIG. 8. Time series of residual heights for (a) 2018 and (c) 2019 after predicted tides have been removed. Also shown are the residuals from the collocated tide gauge (orange). The predicted tides for both GPS-IR and bubbler time series are based on the full bubbler tide gauge series (modern and historical) with the scaling error in the modern data accounted for. The GPS-IR results have had the offset between the 2018 and 2019 data removed prior to plotting. (b),(d) The difference between the GPS-IR and bubbler tide gauge residual heights shown in (a) and (c) for (b) 2018 and (d) 2019. The $\dot{H}$ effect has been removed at this point.

the $\dot{H}$ effect (which is accounted for) but possibly second-order effects such as the interaction of the $\dot{H}$ effect with the tropospheric delay. Löfgren et al. (2014) looked at five sites from around the world and found RMSEs of between 6.2 cm at Onsala (GTGU), Sweden, which has limited tides and rural setting to 43.2 cm at Brest (BRST), France which has a tidal range of over 4 m and a very cluttered local environment. Santamaría-Gómez et al. (2015) studied eight different sites in Europe and Australia with RMSEs a mean of about 11 cm but with no real evidence for a dependence on tidal range. However, the reflector heights were not estimated using the periodogram but using a Kalman filter approach to separate sections of a pass that have a strong reflection signal. Santamaría-Gómez and Watson (2017) compared results from a geodetic-quality receiver and antenna in a normal upright position to a collocated geodetic-quality antenna pointed sideways toward the water at Spring Bay, Australia (SPBY). They found an RMS of 3 cm for the sideways antenna compared to 10 cm for the traditional setup. They attributed this mainly to improved spectral resolution due to an increased range of elevations where SNR oscillations from the water are dominant, something we also see in this study (Fig. 4). In Fig. 9 we compile RMSEs from published work (Chen et al. 2019; Jin et al. 2017; Larson et al. 2013, 2017; Lee et al. 2019; Löfgren and Haas 2014; Löfgren et al. 2014; Peng et al. 2019; Puente and Valdés 2019; Reinking 2016; Santamaría-Gómez and Watson 2017; Santamaría-Gómez et al. 2015; Song et al. 2019; Zhang et al. 2019; Strandberg et al. 2019; Sun 2017; Vu et al. 2019; Wang et al. 2018a; Wang et al. 2018; Wang et al. 2018b,c, 2019) as a function of tidal range and segregated by the method used to estimate water levels. Boxplots are used at some sites where a publication supplied a range of RMSEs either due to

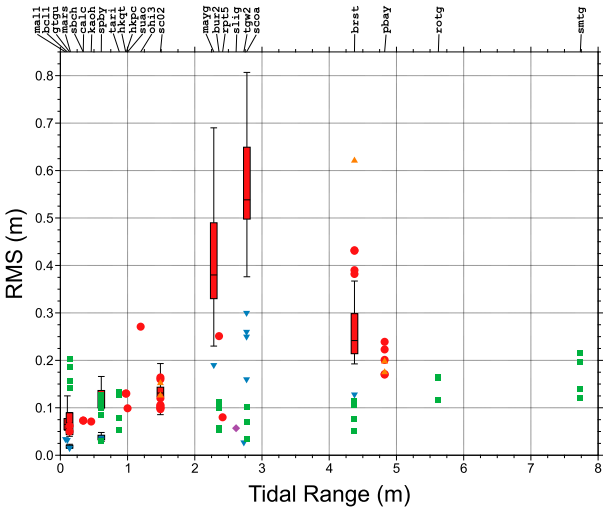

FIG. 9. RMSE as a function of tidal range for GNSS-IR results given in publications. Red dots and boxplots indicate solutions that used the Lomb–Scargle periodogram as the main means of estimating reflector heights. Blue inverted triangles are results that used inverse modeling, least squares, or something else to estimate reflector heights. Green squares indicate that a Kalman filter or similar was used to produce reflector heights from multiple near-simultaneous satellite passes and signals. Orange triangles are where wavelets were used to estimate reflector heights. Boxplots are where multiple estimates of RMSE were published either for individual satellites systems and/or signals or when different strategies were applied. Purple diamond is the result for this experiment. Names at the top are the four-character IDs for the GNSS sites. Names Suao and Kaoh have been given to the two GNSS sites, Suao and Kaohsiung, in Taiwan used in Lee et al. (2019).

analyzing each frequency and satellite system separately (e.g., Wang et al. 2019) or to variations in the method such as different elevation ranges (Wang et al. 2018a), presmoothing of the SNR signal (Zhang et al. 2019; Wang et al. 2018a), for example. For those studies that simply used the periodogram on individual satellite passes (red circles and boxplots) we see an obvious increase in RMSE as a function of tidal range which is significant at the 3σ level. Our results with an RMSE of 5.7 cm at Sligo and tidal range of 2.6 m, which also use this methodology, is significantly below the predicted curve. The results from Santamaría-Gómez and Watson (2017) and Santamaría-Gómez et al. (2015) which uses a Kalman filter approach to estimate individual reflector heights (green squares) appears to have less of a dependence on tidal range (as mentioned above) but perhaps a slightly larger intercept 9 ± 1 cm (compared to the periodogram at approximately 7 ± 2 cm). Finally, those publications that estimate water levels by combining multiple satellite passes, generally within a certain window, (blue triangles) also appear to have a tidal range dependence similar to the periodogram approach but there are less data to be confident of this. Also note the very low RMSE blue boxplots for GTGU and SPBY from Strandberg et al. (2016), which used a Kalman filter/B-spline approach to get evenly sampled GNSS-IR derived water levels. Although the technique looks promising and can be applied to the low-cost antenna dataset it has only been done at sites with very low tidal ranges. At Spring Bay Santamaría-Gómez and Watson (2017) achieved an RMSE of around 3 cm with a sideways-mounted antenna compared to our 5.7 cm. However, the tidal range at Spring Bay is much smaller than at Sligo so that could be the main factor in the higher precision. Therefore, we cannot say at this point whether the precision is also from mounting the low-cost antenna sideways and oriented toward the water or the lack of immunity to multipath in the low-cost antenna is the main cause.

Our result, with a low-cost receiver, is therefore equal to if not better than a traditional geodetic-quality setup with a zenith-oriented antenna. Given this demonstration it is easy to speculate that the same setup can be used for other reflectometry applications traditionally served by geodetic-quality receivers such as soil-moisture and snow-depth estimation (Larson 2019). Indeed, given the relatively low cost of the system one can imagine a whole suite of possible experiments that would otherwise be prohibitively expensive. The situation is also only going to improve further. There are already low-cost chips that are multifrequency and multisystem which will increase dramatically the amount of data available. Of course, the GPS receiver is not the only equipment required to run the system. Power, networking, logging, cabling, and containers are also required. Our first setup cost on the order of $150 (U.S. dollars), and the second, with the addition of wireless networking and the cost of a GPS development kit, took the total to around $500 (U.S. dollars). Neither set ups required renewable power or a datalogger. However, compared to the cost of a conventional geodetic receiver or a tide gauge installation this is still low cost.

There are of course also downsides to the low-cost system. One advantage of a geodetic-quality GNSS-IR tide gauge is that alongside measuring the water level it is also measuring its position very accurately. This allows you to estimate any vertical land movement at the gauge and tie the measurements into a global reference frame such as ITRF2014 (Altamimi et al. 2016). This means the water-level measurements are essentially absolute rather than relative and more directly comparable with satellite altimetry data. Positioning accuracy with a low-cost system is generally a few orders of magnitude worse than a geodetic-quality system at around 2–3 m mainly due to the poor multipath suppression, a gain pattern that is highly irregular (Pesyna et al. 2015) and no access to phase observations. However, there is much interest in developing high precision positioning from smartphones and low-cost hardware, particularly following the release of the Android Nougat (version 7) operating system for mobile devices which allowed raw GNSS data logging (Malkos 2016). With this, precise positioning at subcentimeter accuracy is achievable (Realini et al. 2017; Geng and Li 2019) particularly if the positioning is realized through double differencing to a nearby Continuously Operating Reference Station (CORS). Recently, Knight et al. (2020) presented some results from a low-cost GNSS buoy platform. They used a single-frequency GNSS receiver and obtained an RMSE of 1.4 cm when compared to a nearby tide gauge. This was accomplished using double differencing to a CORS 200 m away and adding a ground plane to

the antenna to suppress multipath. It is therefore possible to see low-cost positioning methods improve in accuracy sufficiently to tie into a reference frame in the very near future.

At the present time this technology is not sufficiently developed to replace traditional high-accuracy tide gauge systems that are capable of resolving water elevations to 1 cm or better but we have shown here that they can act as a very useful independent cross check for data quality and may be suitable for some stand-alone applications where slightly lower accuracy and an inherent temporal averaging of results can be tolerated.

Acknowledgments. The project was funded by the Natural Environment Research Council (NERC) through the Innovation Grant Programme under Grant NE/R00949X/1. The program seeks opportunities to apply existing research into new areas, providing the seed funding to increase and accelerate the uptake and impact of U.K.-funded research. This work was also partially funded by the Natural Environment Research Council (NERC) as part of a National Capability, Official Development Assistance award (NC-ODA), NE/R000123/1. Many thanks to the Royal National Lifeboat Institution (RNLI) for their support for this project. In particular, thanks are due to Jon Oxenham for supporting the development of the proposal, suggesting the experimental site, and enabling the project to conduct the experiments in association with the RNLI, and later to Samantha Norman for succeeding Jon in that role. Huge thanks also to Willie Murphy and all the crew at RNLI Sligo for their unwavering enthusiasm, help, and support for the project, providing space for and help with the installation, and ongoing maintenance of the systems. We are also grateful for the kind support for early work on opportunistic proof-of-concept deployments of GPS receivers within coastal radar installations at Thorpeness, United Kingdom, under Project NE/M021653/1; and at Crosby, United Kingdom, from Cai Bird and Alex Sinclair at Marlan Maritime Technologies Ltd.

Data availability statement. The raw SNR data collected at Sligo over the 2018–19 period used in this paper are archived at doi:10.5281/zenodo.3726741. A full description of the datasets is provided along with the data. Tide gauge data are courtesy of Marine Ireland and can be downloaded from their data center (https://www.marine.ie/Home/site-area/data-services/marine-data-centre). Alternatively tide gauge data for Sligo can be downloaded from EMODnet Physics (https://www.emodnet-physics.eu/Portal/).

REFERENCES

Altamimi, Z., P. Rebischung, L. Métivier, and X. Collilieux, 2016: ITRF2014: A new release of the International Terrestrial Reference Frame modeling nonlinear station motions. *J. Geophys. Res. Solid Earth*, **121**, 6109–6131, https://doi.org/10.1002/2016JB013098.

Axelrad, P., C. J. Comp, and P. F. Macdoran, 1996: SNR-based multipath error correction for GPS differential phase. *IEEE Trans. Aerosp. Electron. Syst.*, **32**, 650–660, https://doi.org/10.1109/7.489508.

Bilich, A., P. Axelrad, and K. Larson, 2007: Scientific utility of the signal-to-noise ratio (SNR) reported by geodetic GPS receivers. *Proc. 20th Int. Tech. Meeting of the Satellite Division of the Institute of Navigation*, Fort Worth, TX, Institute of Navigation, 1999–2010.

Böhm, J., B. Werl, and H. Schuh, 2006: Troposphere mapping functions for GPS and very long baseline interferometry from European Centre for Medium-Range Weather Forecasts operational analysis data. *J. Geophys. Res.*, **111**, B02406, https://doi.org/10.1029/2005JB003629.

——, G. Möller, M. Schindelegger, G. Pain, and R. Weber, 2014: Development of an improved empirical model for slant delays in the troposphere (GPT2w). *GPS Solutions*, **19**, 433–441, https://doi.org/10.1007/s10291-014-0403-7.

Chen, F. D., L. L. Liu, and F. Guo, 2019: Sea surface height estimation with multi-GNSS and wavelet de-noising. *Sci. Rep.*, **9**, 15181, https://doi.org/10.1038/S41598-019-51802-9.

Elosegui, P., J. L. Davis, R. T. K. Jaldehag, J. M. Johansson, A. E. Niell, and I. Shapiro, 1995: Geodesy using the global positioning system: The effects of signal scattering on estimates of site position. *J. Geophys. Res.*, **100**, 9921–9934, https://doi.org/10.1029/95JB00868.

Foreman, M. G. G., and R. F. Henry, 1989: The harmonic analysis of tidal model time series. *Adv. Water Resour.*, **12**, 109–120, https://doi.org/10.1016/0309-1708(89)90017-1.

——, and E. Neufeld, 1991: Harmonic tidal analyses of long time series. *Int. Hydrogr. Rev.*, **68**, 85–108.

——, J. Y. Cherniawsky, and V. A. Ballantyne, 2009: Versatile harmonic tidal analysis: Improvements and applications. *J. Atmos. Oceanic Technol.*, **26**, 806–817, https://doi.org/10.1175/2008JTECHO615.1.

Geng, J. H., and G. C. Li, 2019: On the feasibility of resolving Android GNSS carrier-phase ambiguities. *J. Geod.*, **93**, 2621–2635, https://doi.org/10.1007/s00190-019-01323-0.

Georgiadou, Y., and A. Kleusberg, 1988: On carrier signal multipath effects in relative GPS positioning. *Manuscr. Geod.*, **13**, 172–179.

Haigh, I. D., and Coauthors, 2020: The tides they are a-changin': A comprehensive review of past and future nonastronomical changes in tides, their driving mechanisms, and future implications. *Rev. Geophys.*, **58**, e2018RG000636, https://doi.org/10.1029/2018RG000636.

IOC, 2006: Manual on sea level measurements and interpretation. IOC Manuals and Guides 14, Vol IV, 87 pp., https://library.wmo.int/doc_num.php?explnum_id=9328.

Jin, S., X. Qian, and X. Wu, 2017: Sea level change from BeiDou Navigation Satellite System-Reflectometry (BDS-R): First results and evaluation. *Global Planet. Change*, **149**, 20–25, https://doi.org/10.1016/j.gloplacha.2016.12.010.

Knight, P. J., C. O. Bird, A. Sinclair, and A. J. Plater, 2020: A low-cost GNSS buoy platform for measuring coastal sea levels. *Ocean Eng.*, **203**, 107198, https://doi.org/10.1016/j.oceaneng.2020.107198.

Larson, K. M., 2019: Unanticipated uses of the global positioning system. *Annu. Rev. Earth Planet. Sci.*, **47**, 19–40, https://doi.org/10.1146/annurev-earth-053018-060203.

——, J. S. Lofgren, and R. Haas, 2013: Coastal sea level measurements using a single geodetic GPS receiver. *Adv. Space Res.*, **51**, 1301–1310, https://doi.org/10.1016/j.asr.2012.04.017.

——, R. D. Ray, and S. D. P. Williams, 2017: A 10-year comparison of water levels measured with a geodetic GPS receiver versus a conventional tide gauge. *J. Atmos. Oceanic Technol.*, **34**, 295–307, https://doi.org/10.1175/JTECH-D-16-0101.1.

Lee, C. M., and Coauthors, 2019: Evaluation and improvement of coastal GNSS reflectometry sea level variations from existing GNSS stations in Taiwan. *Adv. Space Res.*, **63**, 1280–1288, https://doi.org/10.1016/j.asr.2018.10.039.

Löfgren, J. S., and R. Haas, 2014: Sea level measurements using multi-frequency GPS and GLONASS observations. *EURASIP J. Adv. Signal Process.*, **2014**, 50, https://doi.org/10.1186/1687-6180-2014-50.

——, ——, and H. G. Scherneck, 2014: Sea level time series and ocean tide analysis from multipath signals at five GPS sites in different parts of the world. *J. Geodyn.*, **80**, 66–80, https://doi.org/10.1016/j.jog.2014.02.012.

Lomb, N. R., 1976: Least-squares frequency analysis of unequally spaced data. *Astrophys. Space Sci.*, **39**, 447–462, https://doi.org/10.1007/BF00648343.

Malkos, S., 2016: User location takes center stage in new Android OS: Google to provide raw GNSS measurements. *GPS World*, **27**, 36, https://www.gpsworld.com/google-to-provide-raw-gnss-measurements/.

Martín Míguez, B., L. Testut, and G. Wöppelmann, 2008: The Van de Casteele test revisited: An efficient approach to tide gauge error characterization. *J. Atmos. Oceanic Technol.*, **25**, 1238–1244, https://doi.org/10.1175/2007JTECHO554.1.

——, ——, and ——, 2012: Performance of modern tide gauges: Towards mm-level accuracy. *Sci. Mar.*, **76**, 221–228, https://doi.org/10.3989/scimar.03618.18A.

Müller, M., B. K. Arbic, and J. X. Mitrovica, 2011: Secular trends in ocean tides: Observations and model results. *J. Geophys. Res.*, **116**, C05013, https://doi.org/10.1029/2010JC006387.

Nievinski, F. G., and K. M. Larson, 2014: Forward modeling of GPS multipath for near-surface reflectometry and positioning applications. *GPS Solutions*, **18**, 309–322, https://doi.org/10.1007/s10291-013-0331-y.

Peng, D., E. M. Hill, L. Li, A. D. Switzer, and K. M. Larson, 2019: Application of GNSS interferometric reflectometry for detecting storm surges. *GPS Solutions*, **23**, 47, https://doi.org/10.1007/s10291-019-0838-y.

Pérez, B., A. Payo, D. López, P. L. Woodworth, and E. Alvarez Fanjul, 2014: Overlapping sea level time series measured using different technologies: An example from the REDMAR Spanish network. *Nat. Hazards Earth Syst. Sci.*, **14**, 589–610, https://doi.org/10.5194/nhess-14-589-2014.

Pesyna, K., R. Heath, and T. Humphreys, 2015: Accuracy in the palm of your hand: Centimeter positioning with a smartphone quality GNSS antenna. *GPS World*, **26**, 27–31, https://www.gpsworld.com/accuracy-in-the-palm-of-your-hand/.

Puente, V., and M. Valdés, 2019: Sea level determination in the Spanish coast using GNSS-R. *Proceedings*, **19**, 11, https://doi.org/10.3390/PROCEEDINGS2019019011.

Realini, E., S. Caldera, L. Pertusini, and D. Sampietro, 2017: Precise GNSS positioning using smart devices. *Sensors*, **17**, 2434, https://doi.org/10.3390/s17102434.

Reinking, J., 2016: GNSS-SNR water level estimation using global optimization based on interval analysis. *J. Geod. Sci.*, **6**, 80–92, https://doi.org/10.1515/JOGS-2016-0006.

Santamaría-Gómez, A., and C. Watson, 2017: Remote leveling of tide gauges using GNSS reflectometry: Case study at Spring Bay, Australia. *GPS Solutions*, **21**, 451–459, https://doi.org/10.1007/s10291-016-0537-x.

——, ——, M. Gravelle, M. King, and G. Woppelmann, 2015: Levelling co-located GNSS and tide gauge stations using GNSS reflectometry. *J. Geod.*, **89**, 241–258, https://doi.org/10.1007/s00190-014-0784-y.

Scargle, J. D., 1982: Studies in astronomical time series analysis. II. Statistical aspects of spectral analysis of unevenly spaced data. *Astrophys. J.*, **263**, 835–853, https://doi.org/10.1086/160554.

Song, M., X. He, X. Wang, Y. Zhou, and X. Xu, 2019: Study on the quality control for periodogram in the determination of water level using the GNSS-IR technique. *Sensors*, **19**, 4524, https://doi.org/10.3390/s19204524.

Strandberg, J., T. Hobiger, and R. Haas, 2016: Improving GNSS-R sea level determination through inverse modeling of SNR data. *Radio Sci.*, **51**, 1286–1296, https://doi.org/10.1002/2016RS006057.

——, ——, and ——, 2019: Real-time sea-level monitoring using Kalman filtering of GNSS-R data. *GPS Solutions*, **23**, 61, https://doi.org/10.1007/s10291-019-0851-1.

Sun, J., 2017: Ground-based GNSS-reflectometry sea level and lake ice thickness measurements. Ph.D. thesis, Ohio State University, 111 pp.

Vu, P. L., and Coauthors, 2019: Identifying 2010 Xynthia storm signature in GNSS-R-based tide records. *Remote Sens.*, **11**, 782, https://doi.org/10.3390/rs11070782.

Wang, N. Z., T. H. Xu, F. Gao, and G. C. Xu, 2018: Sea level estimation based on GNSS dual-frequency carrier phase linear combinations and SNR. *Remote Sens.*, **10**, 470, https://doi.org/10.3390/rs10030470.

Wang, X., Q. Zhang, and S. Zhang, 2018a: Water levels measured with SNR using wavelet decomposition and Lomb–Scargle periodogram. *GPS Solutions*, **22**, 22, https://doi.org/10.1007/s10291-017-0684-8.

——, ——, and ——, 2018b: Sea level estimation from SNR data of geodetic receivers using wavelet analysis. *GPS Solutions*, **23**, 6, https://doi.org/10.1007/s10291-018-0798-7.

——, ——, and ——, 2018c: Azimuth selection for sea level measurements using geodetic GPS receivers. *Adv. Space Res.*, **61**, 1546–1557, https://doi.org/10.1016/j.asr.2018.01.002.

——, X. He, and Q. Zhang, 2019: Evaluation and combination of quad-constellation multi-GNSS multipath reflectometry applied to sea level retrieval. *Remote Sens. Environ.*, **231**, 111229, https://doi.org/10.1016/j.rse.2019.111229.

Williams, S. D. P., and F. G. Nievinski, 2017: Tropospheric delays in ground-based GNSS multipath reflectometry—Experimental evidence from coastal sites. *J. Geophys. Res. Solid Earth*, **122**, 2310–2327, https://doi.org/10.1002/2016JB013612.

Woodworth, P. L., 2010: A survey of recent changes in the main components of the ocean tide. *Cont. Shelf Res.*, **30**, 1680–1691, https://doi.org/10.1016/j.csr.2010.07.002.

Zhang, S., K. Liu, Q. Liu, C. Zhang, Q. Zhang, and Y. Nan, 2019: Tide variation monitoring based improved GNSS-MR by empirical mode decomposition. *Adv. Space Res.*, **63**, 3333–3345, https://doi.org/10.1016/j.asr.2019.01.046.